Biomolecule-Assisted Synthesis and Electrochemical Hydrogen Storage of Bi_2S_3 Flowerlike Patterns with Well-Aligned Nanorods

Bin Zhang, Xingchen Ye, Weiyi Hou, Yu Zhao, and Yi Xie*

Department of Nanomaterials and Nanochemistry, Hefei National Laboratory for Physical Sciences at the Microscale, University of Science and Technology of China, Hefei 230026, People's Republic of China

Received: February 6, 2006; In Final Form: March 21, 2006

Bi_2S_3 flowerlike patterns with well-aligned nanorods were synthesized using a facile solution-phase biomolecule-assisted approach in the presence of L-cysteine (an ordinary and cheap amino acid), which turned out to serve as both the S source and the directing molecule in the formation of bismuth sulfide nanostructures. Emphatically, no nauseous scent (H_2S) appeared in our experiments, which could not be avoided in other previous reports. The morphology, structure, and phase composition of the as-prepared Bi_2S_3 products were characterized using various techniques (scanning electron microscopy, X-ray diffraction, X-ray photoelectron spectroscopy, transmission electron microscopy, selected area electron diffraction, and high-resolution transmission electron microscopy). The formation mechanism for the bismuth sulfide flowerlike assemblies with well-arranged nanorods was also discussed. In addition, other Bi_2S_3 homogeneous nanostructures (e.g., networklike nanoflakes, nanorod-based bundles, and nanoflakes) were obtained through varying the experimental parameters. Interestingly, we have found that these synthesized bismuth sulfide nanostructures using the biomoleucle-assisted approach could electrochemically charge and discharge with the capacity of 142 (mA h)/g (corresponding to 0.51 wt % hydrogen in single-walled carbon nanotubes) under normal atmosphere at room temperature. A novel two-plateau phenomenon was observed in the synthesized Bi_2S_3 nanostructures, suggesting that there were two independent steps in the charging process. It has been demonstrated that the bismuth sulfide's morphology and the constant charge−discharge current density had a noticeable influence on their capacity of electrochemical hydrogen storage. These differences in hydrogen storage capacity are likely due to the size and density of space/pores as well as the morphology of different Bi_2S_3 nanostructures. The novel Bi_2S_3 nanomaterials may find potential applications in hydrogen storage, high-energy batteries, luminescence, optoelectronic and catalytic fields, as well as in the studies of structure−property relationships. This facile, environmentally benign, and solution-phase biomolecule-assisted method can be potentially extended to the preparation of other metal chalcogenides including FeS, CuS, NiS, PbS, MnS, and CoS nanostructures.

1. Introduction

During the past few decades, much attention has been focused on nanocrystals and one-dimensional (1D) nanostructures of semiconductors, owing to their fundamental significance in investigating the dependence of various physical properties on dimensionality and size reduction as well as their potential applications in the fabrication of electronic, optoelectronic, electrochemical, and electromechanical devices with nanoscale dimensions.[1−4] Among various nanomaterials, metal sulfides have attracted extensive attention for promising applications in many fields.[5−8] A variety of methods, such as sonochemical techniques,[9] template-directed procedures,[10] organometallic complex decomposition,[11−13] electrochemical deposition,[14,15] chemical vapor deposition (CVD),[16] hydrothermal and solvothermal routes,[17−20] and the crystallization of amorphous colloids,[21] have successfully been developed for generating 1D metal sulfides. Although great progress has been achieved on the synthesis approach, present methods usually require high temperature and involve the use of expensive and toxic organic agents and a series of complicated procedures, accompanied by a great amount of pungent H_2S as a result of the employment of familiar sulfur source (thioactamide, thiourea, sodium thiosulfate, Na_2S, or H_2S). Therefore, the necessity of searching for a simple, inexpensive, efficient, and environmentally benign approach arises for the high-throughput production of 1D metal sulfide nanomaterials.

Recently, biomolecule-assisted synthesis methods have been a new and promising focus in the preparation of various nanomaterials where biomolecules have been exploited only as structure-directing agents. Protein cages were adopted as the templates to synthesize nanocrystals.[23,24] Virus, peptide, and lemongrass were utilized as templates to prepare transitional metal nanomaterials.[25−29] Nanoparticles and nanowires of metal sulfide semiconductors have successfully been fabricated and assembled using peptide, virus, bacteria, and fungus in the presence of Na_2S or H_2S.[29−35] These interesting works mainly focused on the preparation and assembly of semiconductor nanoparticles with the assistance of macro-biomolecules that only function as the structure-directing molecules rather than as the sulfur source. For example, it was confirmed that CdS nanoparticles could not form in the absence of sulfur-containing inorganic salts when *Fusarium oxysporum* biomass was adopted.[35] More recently, Komarneni et al. used glutathione (GSH), a large polypeptide molecule, as both the assembling molecule and the sulfur source to synthesize the highly ordered snowflake structure of bismuth sulfide nanorods under microwave irradia-

* Author to whom correspondence should be addressed. Phone/Fax: 86-551-3603987. E-mail: yxie@ustc.edu.cn.

10.1021/jp060769j CCC: $33.50 © 2006 American Chemical Society
Published on Web 04/19/2006

tion.[36] This thought-provoking work inspires us to explore a simpler and more economical method to prepare metal sulfides using small biomolecules. Thus, L-cysteine ($HSCH_2CH(NH_2)$-COOH) has attracted researchers' attention because of its simple hydrosulfide-group-including structure. In a recent communication, Qian and co-workers synthesized antimony sulfide nanowires in the presence of cysteine.[37] Cysteine and glutathione have also been used to prepare biostabilized CdS nanoparticles,[38] where the band gap energies could be adjusted by varying the pH value, the biomolecules, and their corresponding concentrations. Very recently, we have also synthesized the porous spongelike Ni_3S_2 nanostructures on Ni foil substrate with high electrochemical activity in the presence of cysteine.[39] Thus, it would be interesting to develop a simple L-cysteine-assisted biological approach to prepare other sulfide nanomaterials, especially with a novel homogeneous self-assembly pattern of 1D semiconductor nanostructures.

In this work, bismuth sulfide (Bi_2S_3) was chosen as an example to investigate the biomolecule-assisted synthesis of metal sulfides, not only due to its utilization in photodiode arrays and photovoltaic converters[9] but also wide applications in thermoelectric cooling technologies based on the Pelitier effect.[9,12] In addition, bismuth sulfide is a well-known material with a lamellar structure[16,39] and thus may exhibit excellent electrochemical hydrogen storage properties, as other fullerene-like materials (e.g., carbon nanotube (CNT) and MoS_2 nanotubes).[41−48] Herein, a facile biological approach was developed to fabricate Bi_2S_3 homogeneous flowerlike patterns with well-arranged nanorods using L-cysteine, a small, ordinary, and cheap amino acid, as both the S source and the directing molecule under hydrothermal conditions. Other interesting Bi_2S_3 nanostructures (e.g., networklike nanoflakes, nanorod bundles, nanoflakes, and nanorods) have been synthesized through the adjustment of the pH value of the reaction solution, the reaction temperature, and the ratio of $Bi(NO_3)_3$ to L-cysteine. Emphatically, no nauseous scent (H_2S) appeared in our experiments, which could not be avoided in previous reports. To the best of our knowledge, there have been no reports on the similar small-biomolecule-assisted preparation of single-crystalline Bi_2S_3 nanostructures employing cysteine as both the S source and the capping molecule. The electrochemical hydrogen storage behaviors of these Bi_2S_3 nanostructures were studied. It was found that the morphology exerted a remarkable effect on the electrochemical hydrogen storage behaviors of such nanomaterials. In addition, our study opens a novel and environmentally friendly biological route to the fabrication of other chalcogenide nanostructures and may be conducive to obtain a good knowledge of the dependence of various properties of nanomaterials on their morphology.

2. Experimental Section

2.1. Chemicals. All of the chemicals were of analytical grade and were used as received. Aqueous solutions were prepared using distilled water.

2.2. Synthesis. In a typical procedure, 0.485 g of $Bi(NO_3)_3 \cdot 5H_2O$ and 0.28 g of L-cysteine were first added to 10 mL of distilled water, and the mixture was dispersed to form a homogeneous solution under constant strong stirring. The resulting solution was transferred into a 15 mL Teflon-lined autoclave. The autoclave was sealed, maintained at 150 °C for 24 h, and cooled to room temperature naturally. The black precipitate was collected and washed three times with absolute ethanol and water, respectively. Then the sample was dried in a vacuum at 50 °C for 6 h.

2.3. Characterization. The X-ray diffraction (XRD) patterns of the products were recorded with Rigaku Dmax Diffraction System using a Cu Kα source ($\lambda = 0.154178$ nm). The scanning electron microscopy (SEM) images were taken with a JEOL-JSM-6700F field emission scanning electron microscope (15 kV). Transmission electron microscopy (TEM) images and electron diffraction patterns were obtained with a Hitachi 800 system at 200 kV. The high-resolution transmission electron microscopy (HR-TEM) images and the corresponding selected area electron diffraction (SAED) patterns were taken on a JEOL 2010 high-resolution transmission electron microscope performed at 200 kV. The specimens of TEM and HR-TEM measurements were prepared via spreading a droplet of ethanol suspension onto a copper grid, coated with a thin layer of amorphous carbon film, and allowed to dry in air. A Fourier transform infrared (FTIR) spectroscopic study was carried out with a MAGNA-IR 750 (Nicolet Instrument Co.) FTIR spectrometer. The as-prepared product-containing solution was directly dried in a vacuum at 50 °C to get rid of water, and then a thick film of sample was prepared employing a mixture of KBr and the sample. X-ray photoelectron spectroscopy (XPS) on the products was performed using a ESCALAB MK II X-ray photoelectron spectrometer and non-monochromatized Al−Mg Kα X-rays as the excitation source.

2.4. Electrochemical Measurements. The electrochemical measurements were carried out following the method reported in ref 43 with slight modification. Briefly, the electrode was fabricated by directly pressing the synthesized bismuth sulfide powders on a sheet of nickel foam at 50 MPa. All of the experiments were performed in a three-electrode cell in 5 M KOH at 25 °C under normal atmosphere. The Bi_2S_3 nanostructures were used as the working electrode, $Ni(OH)_2$/NiOOH as the counter electrode, and Hg/HgO as a reference electrode. The Bi_2S_3 nanostructures electrode was charged for 3 h at a current density after a 2 s rest. All of the electrochemical hydrogen storage experiments were carried out using the Land battery system (CT2001A) at room temperature. The cyclic voltammetry measurements were carried out by an electrochemical workstation (CHI 660).

3. Results and Discussion

3.1. Characterization of the Bi_2S_3 Flowerlike Patterns with Well-Aligned Nanorods. The product was first checked using field emission scanning electron microscopy (FESEM), and its typical FESEM images are displayed in Figure 1. From the low-magnification FESEM image, the as-prepared sample is composed of flowerlike patterns (Figure 1a). The high-magnification FESEM reveals that each bud in these patterns is formed through parallel-arranged assembly of many nanorods. The as-prepared bismuth sulfide nanorods in the biological approach were compactly arranged with a budlike shape, and then these nanorod-based buds further assemble into flowerlike patterns, different from the urchinlike patterns of Bi_2S_3 nanorods prepared via a rapid polyol process[19] and the flowerlike Bi_2S_3 nanostructures synthesized with the assistance of thermogravimetric analysis (TGA) where the flowerlike structure consisted of several nanorods with no special assembly.[20] The unique self-support homogeneous pattern may have unique properties and help to understand the dependence of physical and chemical properties of nanomaterials on their morphologies.

X-ray diffraction and X-ray photoelectron spectroscopy were adopted to analyze the crystal structure and phase composition of the products. As shown in Figure 2a, all of the diffraction peaks can be indexed to an orthorhombic phase of Bi_2S_3 with

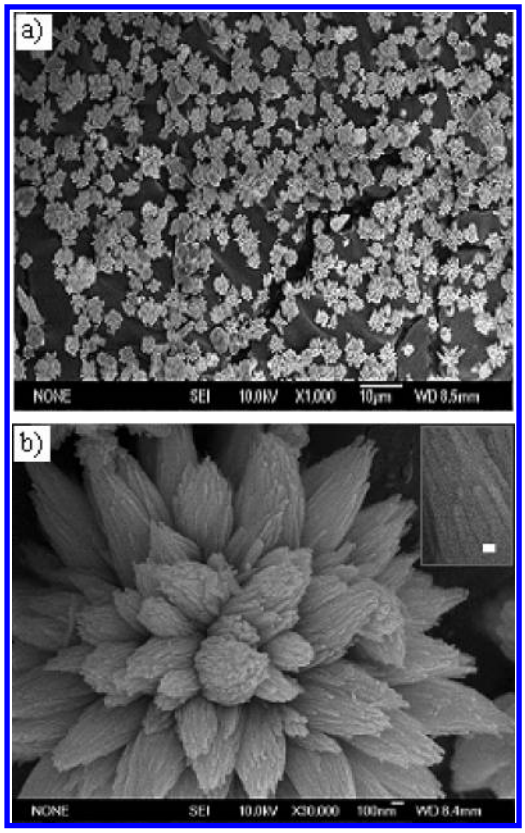

Figure 1. Representative FESEM images of as-prepared Bi_2S_3 nanorods: (a) at low magnification; (b) at high magnification, reflecting the flowerlike pattern of well-arranged rods. The higher-magnification image was also inserted in the top right corner (the white scale bar is 50 nm), further indicating the rod structure of the Bi_2S_3 bundles.

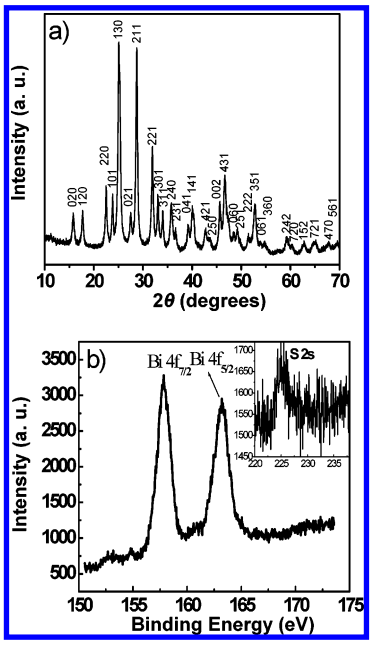

Figure 2. (a) XRD pattern of the as-prepared Bi_2S_3 sample with flowerlike patterns. All of the diffraction peaks can be indexed to an orthorhombic phase of Bi_2S_3. (b) XPS spectra of the as-prepared Bi_2S_3 samples with flowerlike patterns produced at 150 °C, indicating the high purity and the stoichiometric composition of Bi_2S_3.

the calculated lattice constants $a = 10.99$ Å, $b = 11.28$ Å, and $c = 3.980$ Å, which are consistent with the standard values ($a = 11.14$ Å, $b = 11.30$ Å, and $c = 3.981$ Å; Joint Committee on Powder Diffraction Standards Card No. 17-0320). No impurities can be detected in this pattern, which indicates that pure Bi_2S_3 can be obtained under the current synthesis conditions. The XPS spectra of the final product also confirm the stoichiometric composition of Bi_2S_3. The two strong peaks at ca. 158.0 and 163. 2 eV (Figure 2b) can be attributed to Bi $4f_{7/2}$ and Bi $4f_{5/2}$, respectively. The peak at 224.9 eV, appearing in the inset of Figure 2b, can be assigned to the S 2s transition. Taking into account the atomic sensitivity factors of S and Bi, the atomic ratio of Bi/S is approximately 2:3 according to quantification of the peak areas of Bi 4f and S 2s. No peaks of other elements except Bi, S, C, and O are observed in the wide XPS spectrum (not shown here), indicating the high purity of the Bi_2S_3 product.

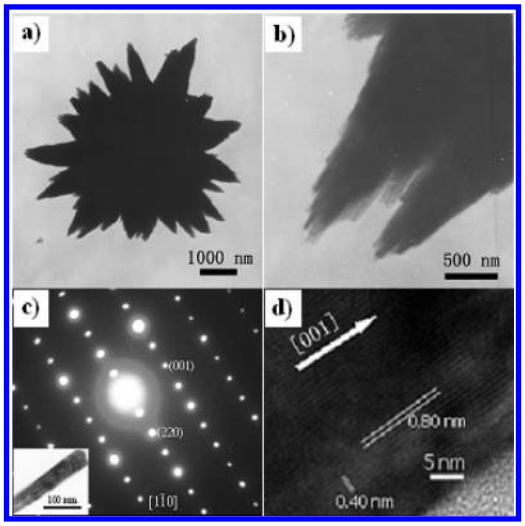

Figure 3. (a) TEM image of one bismuth sulfide flower pattern. (b) Higher-magnification TEM image of one bud in the flowerlike assembly, indexed to the orthorhombic Bi_2S_3 structure. The [1$\bar{1}$0] zone axis of the orthorhombic sample was identified. The inset is associated with the SAED pattern. (d) Corresponding HRTEM image revealing the clear lattice of the rod. The fringes of 0.80 and 0.40 nm were in accordance with the separation between the neighboring lattices of the (110) and (001) planes, respectively.

The morphology and structure of the nanorod-assembled Bi_2S_3 products are further detected by TEM, SAED, and HRTEM. Figure 3a displays the representative TEM image of one Bi_2S_3 flowerlike pattern. The higher-magnification TEM image (Figure 3b) suggests that the bud in these patterns contains many nanorods with a parallel-arranged assembly, confirming the above FESEM observations and also indicating that the flowerlike pattern obtained in the biomolecule-assisted system is obviously different from the familiar urchinlike and flowerlike morphologies.[19,20] Figure 3c shows the TEM image of one bismuth sulfide nanorod existing in the flowerlike assembly and its associated SAED pattern. The index of the spots in the SAED pattern indicates that the nanorod is a single crystal and predominantly grows along the [001] direction (*c*-axis). The conclusion is also supported by the HRTEM observations (Figure 3d), in which the clearly observed lattice fringes reveal that the Bi_2S_3 nanorods in the flowerlike patterns are highly crystalline. The crystal planes, parallel and perpendicular to the rod axis, have spacings of 0.80 and 0.40 nm, which match well with the separations between the neighboring lattices of the (110) and (001) planes, respectively. This result further verifies that the preferential growth occurred along the [001] direction, which is in good agreement with SAED observations. Through extensive investigations on individual nanorods from the Bi_2S_3 products with SAED, we found that this orientation was maintained in all of the products.

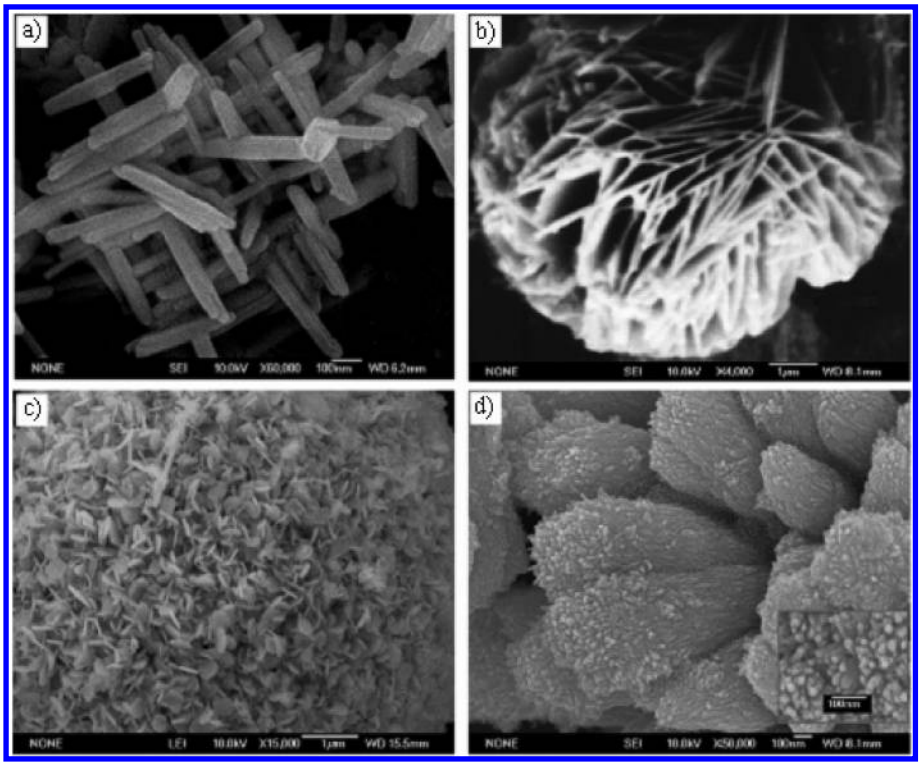

Figure 4. Representative FESEM images of as-prepared Bi_2S_3 samples at different conditions: (a) nanorods prepared from 0.485 g of $Bi(NO_3)_3 \cdot 5H_2O$, 0.28 g of L-cysteine, and 10 mL of H_2O at 150 °C, pH 11; (b) networklike nanoflakes with a thickness of 80−90 nm, prepared from 0.485 g of $Bi(NO_3)_3 \cdot 5H_2O$, 0.28 g of L-cysteine, and 10 mL of H_2O at 120 °C, pH 1; (c) nanoflakes with the thickness of ca. 45 nm, produced from 0.485 g of $Bi(NO_3)_3 \cdot 5H_2O$, 0.15 g of L-cysteine, and 10 mL of H_2O at 150 °C, pH 1; (d) nanorod bundles fabricated from 0.485 g of $Bi(NO_3)_3 \cdot 5H_2O$, 0.35 g of L-cysteine, and 10 mL of H_2O at 150 °C, pH 1. The inset high-magnification FESEM image represents the rod structure of the Bi_2S_3 bundles. The diameter of the rods is ca. 30 nm. The corresponding TEM images of the four as-prepared samples are shown in Figure S1.

TABLE 1: Summary of the Shape, Size, and Pattern of Bi_2S_3 Nanostructues Obtained under Various Conditions

mass of L-cysteine (g)	pH	reaction temperature (°C)	morphology	FESEM image
0.28	1	150	flowerlike patterns with well-arranged nanorods (the rod diameter is ca. 50 nm)	Figure 1b
0.28	11	150	nanorods with a diameter of 60−80 nm (no special pattern)	Figure 4a
0.28	1	120	network-like nanoflakes (the thickness of flake is 80−90 nm)	Figure 4b
0.28	1	200	nanorods with a wide size distribution	not shown
0.15	1	150	nanoflakes (the thickness of the flakes is ca. 45 nm)	Figure 4c
0.35	1	150	nanorod bundles (the rod diameter is about 25 nm)	Figure 4d

3.2. Effects of the Experimental Parameters on the Products' Morphologies. It is found that the pH value of the reaction mixture has an influence on the morphology of the as-prepared Bi_2S_3. When the pH value was regulated to 11 while other conditions remained unchanged, the products were Bi_2S_3 nanorods with a diameter of about 60 nm, as shown in Figure 4a. It can be seen that these rods have not been assembled to form a special morphology, obviously different from Figure 1b. To ascertain the influence factors on the morphology of Bi_2S_3 products, the experimental parameters and their corresponding products' morphologies are displayed in Table 1. Besides, the products' morphologies are very sensitive to the reaction temperature. When the mixture of 0.485 g of $Bi(NO_3)_3 \cdot 5H_2O$, 0.28 g of L-cysteine, and 10 mL of H_2O was maintained at 120 °C for 24 h, networklike nanoflakes with thicknesses of 80−90 nm could be observed, as shown in Figure 4b. When the hydrothermal temperature is increased to 200 °C, the rodlike products with wide size distribution can be seen (not shown here). The great change in the products' morphologies with the reaction temperature reveals that the dynamical crystal growth process is responsible for the formation of the Bi_2S_3 nanostructures, which also indicates that there are different directing functions of cysteine and diverse formation mechanisms at different temperatures. It should be pointed out that a minor amount of nauseous gas (H_2S) is produced when the hydrothermal temperature is above 180 °C.

We have also found that by decreasing the amount of L-cysteine from 0.28 to 0.15 g while other conditions remain unchanged (compared with the condition of Figure 1), the product was Bi_2S_3 nanoflakes, as shown in Figure 4c. These nanoflakes are very small, and their thickness is about 45 nm, lower than that of the networklike nanoflakes shown in Figure 4b. When the amount of cysteine in the reacting mixture was increased to 0.35 g, novel nanobundles could be obtained, and their typical FESEM image is shown in Figure 4d, from which it can be clearly seen that these bundles are comprised of many nanorods with a regular arrangement. A higher-magnification FESEM image further confirms the rodlike shape and demonstrates that the diameter and length of these nanorods are about 30 and 80 nm, respectively. Hence, the successful preparation of novel bismuth sulfide nanostructures reveals that cysteine does not only function as the S source, but also as the size- and shape-controlling agent in the synthesis of Bi_2S_3 nanostructures, and confirms that this method is an efficient way to synthesize novel bismuth sulfide patterns with special assemblies.

3.3. Possible Formation Mechanism of the Synthesized Bi_2S_3 Flowerlike Patterns with Well-Aligned Nanorods. Although the exact mechanism for the bio-assisted formation

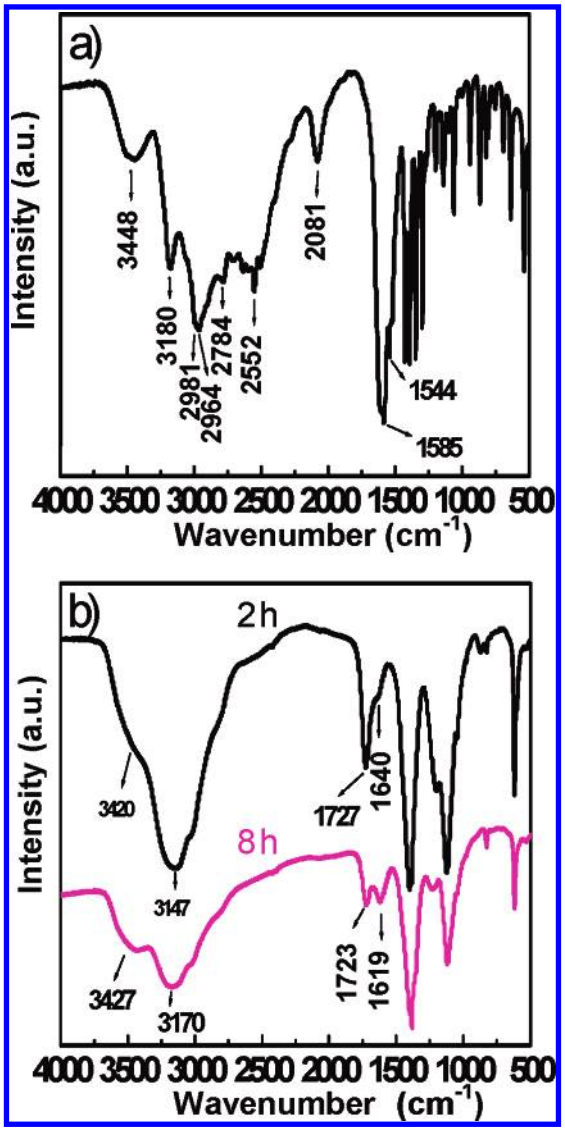

Figure 5. Representative FTIR spectra of (a) pure cysteine and (b) intermediates, including products with different reaction time. Black solid line: 2 h; Magenta short dotted line: 8 h.

of Bi_2S_3 flowerlike patterns with well-aligned nanorods is still under investigation, the coordination interaction between Bi^{3+} and cysteine is undoubtedly significant. In the cysteine molecule, there are many functional groups, such as $-NH_2$, $-COOH$, and $-SH$, which have a strong tendency to coordinate with inorganic cations and metals. The presence of these groups has made cysteine a commonly used self-assembly reagent in the preparation of modified electrodes and biosensors.[49] Burford and coworkers have reported that Bi^{3+} could react with cysteine and glutathione to form complexes on the basis of the observations of mass spectrometry.[50] Therefore, it is reasonable to conclude that bismuth ions can coordinate with cysteine to form initial precursor complexes in our approach. Moreover, it is possible that the amino group reacts with the carboxyl group of the neighboring cysteine molecule to form a dipeptide or polypeptide that can serve as the template to form Bi_2S_3 nanomaterials with various interesting morphologies. Fourier transform infrared studies of the as-prepared Bi_2S_3 also provide preliminary proof for the intermolecular bonding (Figure 5). In comparison with the IR spectrum of pure cysteine (Figure 5a), the frequencies at 1585 and 1544 cm^{-1} (attributed to the characteristic peaks of the I and II bands for amino acids) blueshift to 1727 and 1619 cm^{-1}, which are the diagnostic vibrations of acylamino

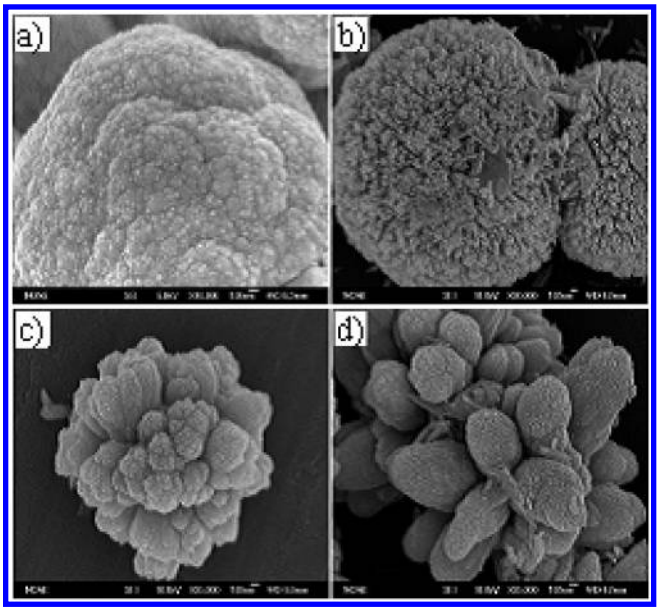

Figure 6. Typical FESEM images of Bi_2S_3 samples with different reaction times: (a) 0.5 h, (b) 1 h, (c) 4 h, (d) 8 h. These samples were prepared from the mixture of 0.485 g of $Bi(NO_3)_3 \cdot 5H_2O$, 0.28 g of L-cysteine, and 10 mL of H_2O at 150 °C. The corresponding TEM images of the intermediates are shown in Figure S2.

($-CO-NH_2-$) I and II bonding, respectively. This manifests the formation of a dimer or polymer of cysteine. The conclusion can also be confirmed by the disappearance of the $-NH_3^+$ signal at ~2082 cm^{-1} in the IR data of the as-prepared sample. Furthermore, in a typical FTIR spectra of the product, we found that the characteristic signal of $-SH$ at ca. 2500 cm^{-1} disappeared after reacting for only 1 h, suggesting that the S component of the product originates from the $-SH$ group of the cysteine molecule. To understand the growth mechanism of the Bi_2S_3 nanostructures accurately, it is necessary to investigate the morphologies of the intermediates involved in the formation. Herein, four samples were collected at different stages in the formation of flowerlike Bi_2S_3 patterns, and their FESEM and TEM images are shown in Figure 6 and Figure S2 of the Supporting Information, respectively. When the hydrothermal reaction was processed for 0.5 h, a spherelike product with many nanoparticles on its surface was observed, as shown in Figure 6a. Figure 6b and Figure S1a of the Supporting Information are the images of the sample reacting for 1 h, revealing that the intermediate after reacting for 1 h was a spherical Bi_2S_3 pattern. Careful observation demonstrates that the sphere was composed of nanorods. When the mixture of Bi^{3+} salt and cysteine was treated for 4 h at 150 °C in the autoclave, the rodlike surface turned into the claviform bundle small flower, as learned from the FESEM image shown in Figure 6c and Figure S1b of the Supporting Information. The formation of the Bi_2S_3 flower is at the expense of small bismuth sulfide nanorods, which may be a typical Ostwald ripening process.[51] When the reaction lasted for 8 h at 150 °C, the as-prepared product is a very rough claviform flower, as displayed in Figure 6d. When the hydrothermal time was increased to 24 h, a beautiful flowerlike Bi_2S_3 pattern with well-arranged rods was observed. (Its corresponding FESEM image is shown in Figure 1b.) The interesting transformation may be attributed to recrystallization along the preferential growth axis to form the rod-composed flower. On the basis of experimental results and discussion, a possible mechanism for the formation of the flowerlike Bi_2S_3 pattern with well-arranged rods is proposed and displayed in Scheme 1.

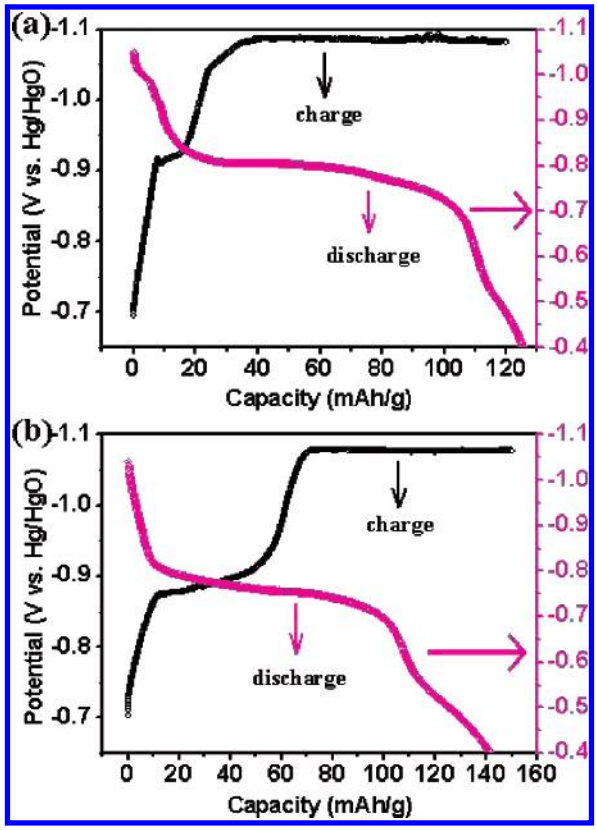

Figure 7. Charge−discharge curves of the obtained Bi_2S_3 nanostructure electrodes at the charge−discharge of 50 mA/g: (a) flowerlike patterns with well-aligned nanorods shown in Figure 1; (b) networklike nanoflakes displayed in Figure 4b.

3.4. Electrochemical Hydrogen Storage Behavior of the Synthesized Novel Bi_2S_3 Nanostructures. It is also observed that Bi_2S_3 nanostructures have good electrochemical hydrogen storage capacities at room temperature. Figure 7 displays the charge−discharge voltage changes of bismuth sulfide nanostructures with different morphologies as a function of capacity at a current density of 50 mA/g at room temperature. In the charging curve of flowerlike Bi_2S_3 patterns with well-arranged nanorods (Figure 7a), one obvious plateau of potential appears at 30 (mA h)/g; a weak but perceptible voltage plateau is also observed in low electrochemical capacity. This indicates that two different hydrogen adsorption sites[48] exist in the synthesized Bi_2S_3 flowerlike pattern; in other words, there are two different electrochemical steps in the charging process. It was assumed that the hydrogen was first adsorbed into the interstitial sites/pores between bismuth sulfide nanorods or buds and then entered into the interlayers of Bi_2S_3 nanorods (the lamellar structure of bismuth sulfide[16,40]). This two-potential-plateau phenomenon in the charge process becomes more obvious in the prepared networklike nanoflake electrode (Figure 7b). But in compactly arranged uniform Bi_2S_3 nanoflakes, only one charging plateau is observed between 10 and 80 (mA h)/g in Figure S3 of the Supporting Information, providing important proof for the above-mentioned assumption. It is believed that the porous/spacing structure of the Bi_2S_3 samples mainly contributes to the differences in the charging process. As shown in Figure 7a, the plateau of the discharging potential is observed at ca. −0.9 V, and the discharging capacity of 125 (mA h)/g can be obtained, which amounts to a hydrogen storage capacity of 0.47 wt % in single-walled carbon nanotubes (SWNTs).[43−48] For the compactly arranged uniform Bi_2S_3 nanoflakes, the

SCHEME 1: Proposed Growth Process for the Formation of Bismuth Sulfide Flowerlike Patterns with Well-Aligned Nanorods.

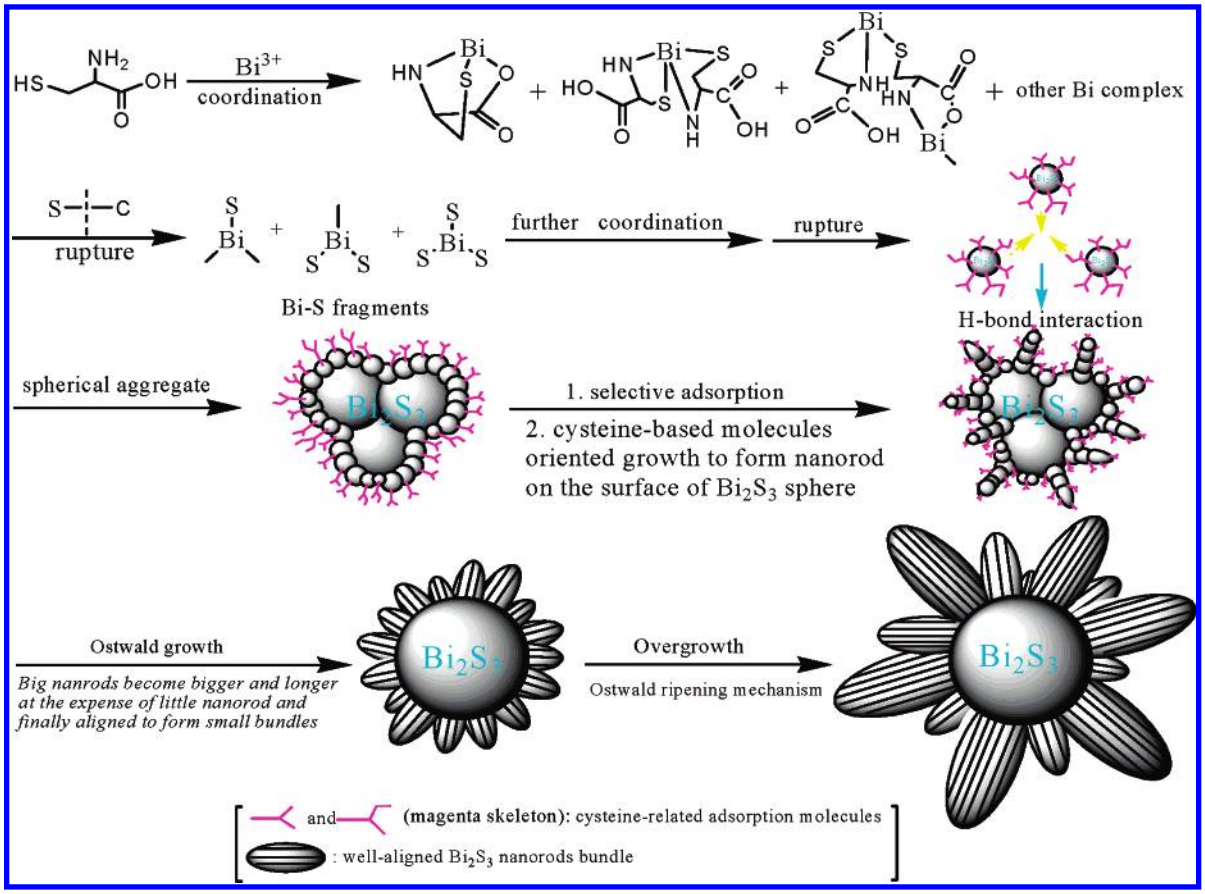

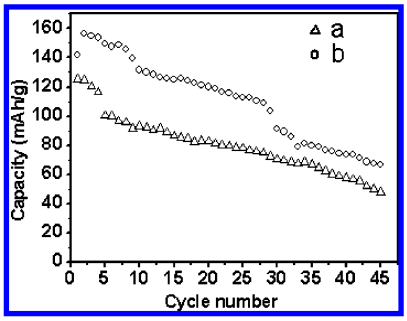

Figure 8. Cycle life of the synthesized flowerlike patterns with (a) well-aligned nanorods and (b) networklike nanoflake electrodes.

discharge capacity decreased to 75 (mA h)/g (Figure S3 of the Supporting Information), revealing that the capacity of electrochemical hydrogen storage of the final products is sensitive to the morphology of bismuth sulfide. When the electrode material was replaced by the networklike sample, the value of the discharging capacity increased to 142 (mA h)/g (0.51 wt % in SWNTs), further confirming that the products' morphologies have exerted a noticeable influence on the capacity of electrochemical hydrogen storage (similar to the Chen's observations on MoS_2 nanotubes[45]). The cycle life of Bi_2S_3 flowerlike patterns with well-aligned nanorods and networklike nanoflake electrodes are shown in Figure 8. After being cycled 45 times at the charge−discharge current density of 50 mA/g, the discharging capacities of flowerlike Bi_2S_3 patterns remain over 45 (mA h)/g, and the discharging capacity of the networklike bismuth sulfide nanoflakes is over 65 (mA h)/g. This indicates that the as-prepared Bi_2S_3 products have a strong resistance against oxidation and corrosion[47] and further manifests that the Bi_2S_3 samples' morphologies are a critical factor to affect their electrochemical hydrogen storage capacities. This indicates that this kind of bismuth sulfide nanostructure may be potentially applied as a material for electrochemical hydrogen storage. The relatively high capacity was considered to be pertinent to the enhanced electro-catalytic activity of the highly porous and layered structures of the synthesized Bi_2S_3 nanomaterials. Note that the discharge capacities of these Bi_2S_3 nanostructures are not very ideal when compared with those of carbon nanotubes and MoS_2 nanotubes at room temperature under ambient atmosphere. However, we believe that the investigations of electrochemical hydrogen storage of Bi_2S_3 nanostructures help us to understand the relationship between morphology and properties and thus inspire us to purposefully synthesize porous or tubular nanostructures with high hydrogen uptake.

Cyclic voltammograms (CVs) were also carried out to further investigate the electrochemical hydrogen adsorption−desorption behaviors of bismuth sulfide nanostructures supported on the porous nickel substrate. In the CV of the porous nickel electrode (Figure S4a in the Supporting Information), one broad oxidation peak of hydrogen is observed at ca. 0.55 V vs Hg/HgO, and one weak desorption peak of hydrogen can be found around −0.92 V, which are typical CV behaviors of foam nickel. When the working electrode was replaced by the flowerlike patterns with well-aligned nanorods, one broad reduction peak of hydrogen is obviously observed at ca. −1.08 V vs Hg/HgO (close to the values of the BN and MoS_2 nanotubes[45,47]), as displayed in Figure 9a. During the following anodic polarization, an anodic multipeak appears at −0.8 V and centers at ca. −0.5 V, which is attributed to the desorption of hydrogen on the Bi_2S_3 patterns. As shown in Figure 9a, the hydrogen desorption peak can be observed prior to the hydrogen oxidation peak, indicating the possible existence of the strong chemisorption of hydrogen,

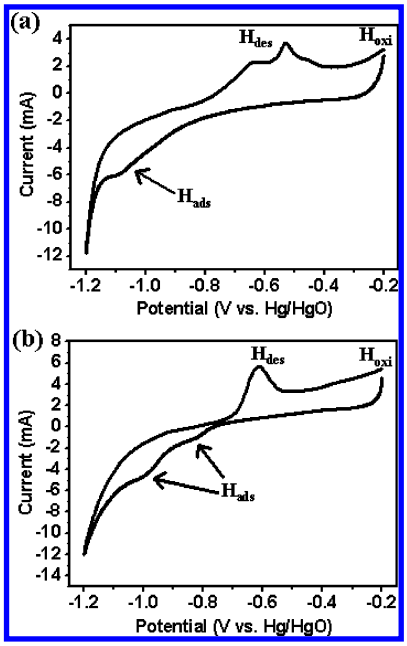

Figure 9. Cyclic voltammograms of the synthesized flowerlike patterns with (a) well-aligned nanorods and (b) networklike nanoflake electrodes. Scan rate: 50 mV/s.

SCHEME 2: Possible Mechanism for the Electrochemical Hydrogen Storge of Bismuth Sulfide Nanostructures

$$Bi_2S_3 + H_2O + e^- \underset{\text{discharge}}{\overset{\text{charge}}{\rightleftharpoons}} (H_{ads} + Bi_2S_3) + OH^-$$

similar to the observations and discussion for CVs of BN nanotubes.[47] Interestingly, two current peaks with peak positions at ca. −0.82 and −0.98 V can be seen in the cathodic segment for the networklike nanoflakes (Figure 9b), suggesting that the two-step adsorption phenomenon of hydrogen in the networklike nanoflakes is more obvious than that of the bismuth sulfide flowerlike nanostructures, and the pores/spaces in the Bi_2S_3 nanostructures are mainly responsible for the first weak voltage plateau in the charging curves. This also provides a complementary explanation for the above discussion on the charging process. It is deemed that the size and density of space or pores as well as the morphologies of different bismuth sulfide nanostructures are responsible for the differences in the electrochemical capacity of hydrogen storage, similar to the discussion of Se microtubes and ultralong Se sub-microtubes.[52,53] As for the charge−discharge mechanism of Bi_2S_3 nanostructures, a simple scheme is proposed in Scheme 2.

4. Conclusions

In summary, a simple hydrothermal method based on a small-biomolecule-assisted technique has been developed to synthesize Bi_2S_3 flowerlike patterns with well-arranged nanorods in a high yield at a low temperature. This route is convenient and environmentally friendly and does not produce the poisonous H_2S gas below 180 °C. The as-prepared Bi_2S_3 nanorods with flowerlike homogeneous assemblies were highly crystalline and grew preferentially along the [001] direction. We demonstrate that cysteine, a simple and inexpensive biomolecule, is not only used as the S source for Bi_2S_3 nanomaterials, but also as an effective morphology-directing molecule. By variation of the ratio of cysteine to bismuth salts, the pH value of the solution, and the reaction temperature, other kinds of Bi_2S_3 homogeneous nanostructures including networklike nanoflakes, nanorod bundles,

nanoflakes, and nanorods were obtained. We have demonstrated that these novel nanomaterials synthesized using the biomolecule-assisted approach can electrochemically charge and discharge with a capacity of 142 (mA h)/g (corresponding to 0.51 wt % hydrogen in SWNTs). It was found that the capacity of electrochemical hydrogen storage is susceptible to the morphology and structure of bismuth sulfide nanostructures. A new two-plateau phenomenon was observed in the synthesized bismuth sulfide nanostructures, suggesting that there were two independent adsorptions/desorptions of hydrogen in the charge process. These novel Bi_2S_3 nanostructures may find potential applications in hydrogen storage, high-energy batteries, luminescence and catalysis fields, as well as the studies of structure−property relationships and the fabrication of nanoscale optoelectronic devices. This simple, environmentally benign, and inexpensive biological route can also be extended to the preparation of other metal chalcogenides (e.g., Sb_2S_3, CuS, NiS, PbS, MnS, and CoS) nanostructures.

Acknowledgment. This work is financially supported by the National Natural Science Foundation of China. B.Z. also thanks Dr. Jiang Wang in Department of Chemistry at USTC for valuable discussion on the electrochemical measurements.

Supporting Information Available: Transmission electron microscopy images of some bismuth sulfide nanostructures obtained at different conditions and the intermediates appearing in the formation of flowerlike patterns with well-arranged assembly, the charge−discharge curves and CV of the obtained Bi_2S_3 uniform nanoflake-supported porous nickel electrode, and the CV of the porous nickel electrode. This material is available free of charge via the Internet at http://pubs.acs.org.

References and Notes

(1) Hu, J.; Odom, T. W.; Lieber, C. M. *Acc. Chem. Res.* **1999**, *32*, 435.
(2) Xia, Y. N.; Yang, P. D.; Sun, Y. G.; Wu, Y. Y.; Mayer, B.; Gates, B.; Yin, Y. D.; Kim, F.; Yan, H. Q. *Adv. Mater.* **2003**, *15*, 353.
(3) Whitesides, G. M.; Grzybowski, B. *Science* **2002**, *295*, 2418.
(4) El-Sayed, M. A. *Acc. Chem. Res.* **2004,** *37*, 326.
(5) Kitova, S.; Eneva, J.; Panov, A.; Haefke, H.; *J. Imaging Sci. Technol.* **1994**, *38*, 484.
(6) Chon, J. W. M.; Zijlstra, P.; Gu, M.; van Embden, J.; Mulvaney, P. *Appl. Phys. Lett.* **2004**, *85*, 5514.
(7) Rao, C. N. R.; Deepak, F. L.; Gundiah, G.; Govindaraj, A. *Prog. Solid State Chem.* **2003**, *31*, 5.
(8) Hu, Y. J.; Chen, F.; Chen, W. M.; Li, X. L. *Adv. Funct. Mater.* **2004**, *14*, 383.
(9) Wang, H.; Zhu, J. J.; Zhu, J. M.; Chen, H. Y. *J. Phys. Chem. B* **2002**, *106*, 3848.
(10) Jiang, T.; Lough, A. J.; Ozin, G. A.; Young, D.; Bendard, R. L. *Chem. Mater.* **1995**, *7*, 245.
(11) Lim, W. P.; Zhang, Z. H.; Low, H. Y.; Chin, W. S. *Angew. Chem., Int. Ed.* **2004**, *43*, 5685.
(12) Boudjouk, P.; Remington, M. P., Jr.; Grier, D. G.; Jarabek, B. R.; McCarthy, G. J. *Inorg. Chem.* **1998**, *37*, 3538.
(13) Waters, J.; Crouch, D.; Raftery, J.; O'Brien, P. *Chem. Mater.* **2004**, *16*, 3289.
(14) Jiang, K. Y.; Wang, Y.; Dong, J. J.; Gui, L. L. *Langmuir* **2001**, *17*, 3635.
(15) Peng, X. S.; Meng, G. W.; Zhang, J.; Zhao, L. X.; Wang, X. F.; Wang, Y. W.; Zhang, L. D. *J. Phys. D: Appl. Phys.* **2001**, *34*, 3224.
(16) Ye, C. H.; Meng, G. W.; Jiang, Z.; Wang, Y. H.; Wang, G. Z.; Zhang, L. D. *J. Am. Chem. Soc.* **2002**, *124*, 15180.
(17) Zhang, L. Z.; Yu, J. C.; Mo, M. S.; Wu, L.; Li, Q.; Kwong, K. W. *J. Am. Chem. Soc.* **2004**, *126*, 8116.
(18) Gao, F.; Lu, Q.; Komarneni, S. *Chem. Commun.* **2005**, 531.
(19) Shen, G. Z.; Chen, D.; Tang, K. B.; Li, F. Q.; Qian, Y. T. *Chem. Phys. Lett.* **2003**, *370*, 334.
(20) Zhang, H.; Yang, D. R., Li, S. Z.; Ji, Y. J.; Ma, X. Y.; Que, D. L. *Nanotechnology* **2004**, *15*, 1122.
(21) Cao, X. B.; Li, L. Y.; Xie, Y. *J. Colloid Interface Sci.* **2004**, *273*, 175.
(22) Sigman, M. B.; Korgel, B. A., Jr. *Chem. Mater.* **2005**, *17*, 1655.
(23) Douglas, T.; Strable, E.; Willits, D.; Aitouchen, A.; Libera, M.; Young, M. *Adv. Mater.* **2002**, *14*, 415.
(24) Douglas, T.; Dichson, D. P. E.; Betteridge, S.; Charnoch, J.; Garner, C. D.; Mann, S. *Science* **1995**, *269*, 54.
(25) Shenton, W.; Douglas, T.; Yong, M.; Stubbs, G.; Mann, S. *Adv. Mater.* **1999**, *11*, 253.
(26) Shankar, S. S.; Rai, A.; Ankamwar, B.; Singh, A.; Ahmad, A.; Sastry, M. *Nat. Mater.* **2004**, *3*, 482.
(27) Knez, M.; Bittner, A. M.; Boes, F.; Wege, C.; Jeske, H.; Maiβ, E.; Kern, K. *Nano. Lett.* **2003**, *3*, 1079.
(28) Reiss, B. D.; Mao, C. B.; Solis, D. J.; Ryan, K. S.; Thomson, T.; Belcher, A. M. *Nano. Lett.* **2004**, *4*, 1127.
(29) Mao, C. B.; Solis, D. J.; Reiss, B. D.; Kottmann, S. T.; Sweeney, R. Y.; Hayhurst, A.; Georgiou, G.; Iverson, B.; Belcher, A. M. *Science* **2004**, *303*, 213.
(30) Labrenz, M.; Druschel, G. K.; Thomsen-Ebert, T.; Gilbert, B.; Welch, S. A.; Kemner, K. M.; Logan, G. A.; Surmmons, R. E.; Stasio, G. D.; Bond, P. L.; Lai, B.; Kelly, S. D.; Banfield, J. F. *Science* **2000**, *290*, 1744.
(31) Dameron, C. T.; Winge, D. R. *Inorg. Chem.* **1990**, *29*, 1343.
(32) Shenton, W.; Pum, D.; Sleytr, U. B.; Mann, S. *Nature* **1997**, *389*, 585.
(33) Mao, C. B.; Flymn, C. E.; Hayhurst, A.; Sweeney, R.; Qi, J.; Georgiou, G.; Iverson, B.; Belcher, A. M. *Proc. Natl. Acad. Sci. U.S.A.* **2003**, *100*, 6946.
(34) Sweeney, R. Y.; Mao, C. B.; Gao, X. X.; Burt, J. L.; Belcher, A. M.; Georgiou, G. G.; Iverson, B. L. *Chem. Biol.* **2004**, *11*, 1553.
(35) Ahmad, A.; Mukherjee, P.; Mandal, D.; Senapati, S.; Khan, M. I.; Kumar, R.; Sastry, M. *J. Am. Chem. Soc.* **2002**, *124*, 12108.
(36) Lu, Q.; Gao, F.; Komarneni, S. *J. Am. Chem. Soc.* **2004**, *126*, 54.
(37) Chen, X. Y.; Zhang, X. F.; Shi, C. W.; Li, X. L.; Qian, Y. T. *Solid State Commun.* **2005**, *134*, 613.
(38) Barglik-Chory, Ch.; Remenyi, Ch.; Strohm, H.; Müller, G. *J. Phys. Chem. B* **2004,** *108*, 7637.
(39) Zhang, B.; Ye, X. C.; Dai, W.; Hou, W. Y.; Xie, Y. *Chem.—Eur. J.* **2006**, *12*, 2337.
(40) Wang, H.; Zhu, J. J.; Chen, H. Y. *J. Phys. Chem. B* **2002**, *106*, 3848.
(41) Tenne, R. *Angew. Chem., Int. Ed.* **2003**, *42*, 5124.
(42) Remkar, M. *Adv. Mater.* **2004**, *16*, 1497.
(43) Dai, G. P.; Liu, C.; Liu, M.; Wang, M. Z.; Cheng, H. M. *Nano. Lett.* **2002**, *2*, 503.
(44) Nützenadel, C.; Züttel, A.; Chartouni, D.; Schlapbach, L. *Electrochem. Solid-State Lett.* **1999**, *2*, 30.
(45) Chen, J.; Kuriyama, N.; Yuan, H.; Takeshita, H. T.; Sakai, T. *J. Am. Chem. Soc.* **2001**, *123*, 11813.
(46) Rajalakshmi, N.; Dhathathreyan, K. S.; Govindaraj, A.; Satishkumar, B. C. *Electrochim. Acta* **2000**, *45*, 4511.
(47) Chen, X.; Gao, X. P.; Zhang, H.; Zhou, Z.; Hu, W. K.; Pan, G. L.; Zhu, H. Y.; Yan, T. Y.; Song, D. Y. *J. Phys. Chem. B* **2005**, *109*, 11525.
(48) Dai, G. P.; Liu, M.; Chen, D. M.; Hou, P. X.; Tong, Y.; Cheng, H. M. *Electrochem. Solid-State Lett.* **2002**, *5*, E13.
(49) Hernández, P.; Vicente, J.; Hernández, L. *Electroanalysis* **2003**, *15*, 1625.
(50) Burford, N.; Eelman, M. D.; Mahony, D. E.; Morash, M. *Chem. Commun.* **2003**, 146.
(51) Krichevsky, O.; Stavans, J. *Phys. Rev. Lett.* **1993**, *70*, 1473.
(52) Zhang, B.; Dai, W.; Ye, X. C.; Hou, W. Y.; Xie, Y. *J. Phys. Chem. B* **2005**, *109*, 22830.
(53) Zhang, B.; Dai, W.; Ye, X. C.; Zuo, F.; Xie, Y. *Angew. Chem., Int. Ed.* **2006**, *45*, 2571.